energies

MDPI

Article

Linear Model of a Turboshaft Aero-Engine Including Components Degradation for Control-Oriented Applications

Teresa Castiglione [1], Diego Perrone [1], Luciano Strafella [2], Antonio Ficarella [2] and Sergio Bova [1,*]

[1] Department of Mechanical Energy and Management Engineering, University of Calabria, 87036 Rende, Italy; teresa.castiglione@unical.it (T.C.)
[2] Department of Engineering for Innovation, University of Salento, 73100 Lecce, Italy
* Correspondence: sergio.bova@unical.it

Abstract: The engine fuel control system plays a crucial role in engine performance and fuel economy. Fuel control, in traditional engine control systems, is carried out by means of sensor-based control methods, which correct the fuel flow rate through correlations or scheduled parameters in order to reduce the error between a measured parameter and its desired value. In the presence of component degradation, however, the relationship between the engine measurable parameters and performance may lead to an increase in the control error. In this research, linear models for advanced control systems and for direct fuel control in the presence of components degradation are proposed, with the main objective being to directly predict and correct fuel consumption in the presence of degradation instead of adopting measurable parameters. Two techniques were adopted for model linearization: Small Perturbation and System Identification. Results showed that both models are characterized by high accuracy in predicting the output engine variables, with the mean errors between model prediction and data below 1%. The maximum errors, recorded for shaft power, were about 6% for Small Perturbation and lower than 3% for System Identification. A simple correlation between engine performance and components degradation was also demonstrated; in particular, the achieved results allow one to conclude that the Small Perturbation approach is the best candidate for controller development when a prediction of components degradation is included.

Keywords: turbo-shaft engine model; gas turbine linear models; compressor degradation; small perturbation; system identification

Citation: Castiglione, T.; Perrone, D.; Strafella, L.; Ficarella, A.; Bova, S. Linear Model of a Turboshaft Aero-Engine Including Components Degradation for Control-Oriented Applications. *Energies* **2023**, *16*, 2634. https://doi.org/10.3390/en16062634

Academic Editors: Roberta De Robbio, Maria Cristina Cameretti and Andrzej Teodorczyk

Received: 30 December 2022
Revised: 2 March 2023
Accepted: 9 March 2023
Published: 10 March 2023

1. Introduction

The aviation industry is committed to reducing emissions and complying with the even more restrictive regulations aimed at reaching the target of net-zero carbon emissions by 2050 [1]. New technologies are being developed to mitigate the impact of the aviation sector on the global climate. To this aim, new ultra-high efficiency and ultra-low emissions aero-propulsion systems, which include, for instance, Ultra High Bypass Ratio (UHBR) engines and Hybrid Electric Propulsion (HEP) [2–4], are being considered by engine manufacturers. These options, however, require major design changes in aircrafts, and are only viable as long-term solutions. In the short-term, strategies for optimizing flight routes for minimum emissions, for improving maintenance schedules and other operational measures, are being adopted. In addition, the use of alternative fuels, the so-called sustainable aviation fuels (SAF), which encompass bio and synthetic fuels, are currently the most viable option in achieving future emission goals and contributing to lowering the dependency on fossil fuels [5]. However, if improvements in the engine components design and development and the use of alternative fuels are necessary to guarantee the achievement of such ambitious targets, the development of advanced engine control systems to satisfy the requirements of the more complex engine architectures operating with the new fuels safely and efficiently will be a fundamental contribution [6,7].

Traditionally, the control system has the function of providing the desired thrust, and guaranteeing that the engine operates within safe boundaries. The fuel flow rate, therefore, needs to be tuned in order to achieve the desired power, and to satisfy the various control modes simultaneously. To fulfil these requirements, min-max control strategies are usually adopted. Moreover, by means of gain scheduling, the controller parameters are tuned at different operating points in such a way that the desired performance characteristics can be achieved over the whole flight envelope [8]. The control of thrust, inlet temperature of high-pressure turbine and surge margins is usually made in an indirect way, by means of measurable parameters such as shaft speeds and pressure [9,10]; thus, a significant number of sensors are installed in the engine. This approach requires a complex architecture [11], and is characterized by a heavy computational burden that arises from multiple iterative control loops [12]. To overcome these limitations and to improve engine performance, modern control methodologies are being developed.

Novel control concepts, known as model-based control (MBC), aim at achieving the direct control of unmeasurable performance parameters through on-line model outputs instead of adopting feedback sensor data [13,14]. Among the various approaches, great attention is being paid to Model Predictive Control (MPC), which is attracting significant attention in all those fields where increasing energy efficiency is required [15], and in particular, to aircraft engines [16–18]. Montazeri et al. [6] developed a turbofan engine control system based on an MPC approach. They first developed a thermodynamic non-linear engine model, which was linearized for model predictive controller application. They demonstrated that the controller satisfies all of the engine constraints, and confirmed successful software and hardware implementation of the control algorithm in real-time. Pang et al. [19] developed a non-linear state-space model for MPC, which, differently from [6], applied an extended Kalman filter every sampling instant, and was based on a quadratic constrained problem rather than a higher-order nonlinear problem. Simulation results demonstrated that this approach allows one to achieve smaller control errors than the standard model predictive control algorithm does, but also that the proposed controller is more time-saving than the standard model predictive control (about 61%). In this context, the development of reliable control-oriented on-board models plays a fundamental role.

In this regard, several approaches to on-board control-oriented engine modeling were investigated for MPC algorithms. These can be classified into non-linear and linear approaches. Among the non-linear approaches, real-time component-level modeling (CLM) uses the physical laws governing the system to derive the mathematical model of the aero-engine. Several models based on CLM were developed over years, and can be found in [20–22]. A full description, including the dynamic equations of all the engine components, can be found in Montazeri et al. [6]. However, owing to the complex involved dynamics, the development of a thorough and precise mathematical model of an aero-engine is generally very challenging. Therefore, alternative approaches, based on data-driven modeling methods, are gaining popularity in the aero-engine community [23]. In particular, artificial intelligence algorithms are currently widely utilized for engine real-time modeling and simulations [24,25]. However, these approaches usually rely on a large amount of data training, and the computational complexity is usually high. Moreover, from a control point of view, the implementation of a non-linear model always results in a non-linear constrained problem to be optimized [17,26]. On the contrary, the adoption of linear real-time models of the engine generates a quadratic constrained problem, which allows one to achieve an optimal solution with less computational effort in comparison to non-linear formulations [27–29]. In addition, a large number of control methods are based on linear control theory. It is, therefore, convenient to deal with linear models, provided that they are sufficiently accurate. These linear models are often obtained by linearization procedures applied to non-linear models.

Several approaches to develop linear models can be found in the literature. The most common approach for the derivation of a linearized model around an equilibrium condition is based on small input and state perturbations [30]. These models adequately capture the

system dynamics near the operating condition, and are valid in a neighborhood of an operating point in certain flight conditions. However, they deviate in accuracy during transients of the system away from equilibrium. To overcome these limitations, Chung et al. [31] presented an analytical method to linearize the engine equations in each time step, and extracted a precise linear model to be used for controller design. When large amounts of experimental data are available instead of a non-linear thermodynamic model, System Identification can be adopted to derive a linear model [32,33]. A comprehensive study about the accuracy of different numerical methods adopted to perform the linearization of the thermodynamic non-linear model of a turbofan engine can be found in Montazeri et al. [34]. The results showed that the linear models obtained from system identification and central difference perturbation methods have higher percentages of compliance compared to the others. However, it is worth pointing out that in the analyzed cases, the on-board modelling and linearization of gas turbine aero-engines was developed for nominal engines, which represent new or clean engine performance.

Control-oriented on-board engine modeling cannot ignore engine components degradation. In fact, due to the normal aging in gas turbine aero-engines with increasing flight cycles, the engine performance deviates from its nominal state; in particular, unmeasured safety-critical parameters such as thrust, surge margin and turbine entry temperature are strongly affected by the engine health status. Therefore, on-board clean engine models cannot predict the control variables of degraded engines correctly, with adverse effects on controller reliability. Degraded engines on-board modeling is, therefore, strongly motivated. A few studies regarding the inclusion of degradation effects in engine models can be found in the literature; however, the majority of this research focused on the adoption of non-linear engine models and require a great amount of data, which burden the on-line computation. Models based on using a Kalman filter for the estimation of engine degradation parameters, aimed at tuning the piecewise linear model to match the degraded engine, can be found in [35–37]. Recently, Wei et al. [7] proposed a novel Hybrid Wiener Model (HWM), which takes into account the degradation effects using post-flight data. Sun et al. [8] included the degradation effects in a non-linear component-level model by means of degradation parameters such as efficiency and flow capacity indexes, and proposed an approach for controller adjustment to deal with degradation implications by developing an industrial min-max control strategy.

In the present study, the possibility of including the effects of engine components degradation directly into the linear model coefficients was investigated. The novel contribution relies on the estimation of the linear model coefficients as a function of components degradation, in order to extrapolate, if any, a simple correlation law. This would allow the achievement of 'real-time' corrections for direct fuel control and improved engine response in the presence of degradation. Therefore, the control objective of the proposed model is to predict the specific fuel consumption directly instead of adopting measurable parameters. In particular, two linearization techniques were evaluated: small perturbation and system identification state-space models. In both cases, the study considered only compressor degradation, evaluated in terms of compressor efficiency and flow coefficient, and analyzed the matrices of the linear model for different degradation values estimated through the monitoring system. The research was developed in the framework of an EU-funded wider project, whose final goal is to define engine controllers that take into account the natural degradation of all engine components simultaneously.

2. Materials and Methods

In order to develop an accurate control-oriented engine linear model that takes into account component degradation, a comprehensive physics-based thermodynamic model was built using the component-level modeling approach. The non-linear model results were adopted for linearization purposes. In particular, two methodologies were proposed for model linearization: Small Perturbations [38,39] and System Identification [40–42] state-space models. Both approaches were applied to the engine model, with inclusion of a certain level of components degradation, and the linear coefficients as a function of component degradation were estimated in order to evaluate the possibility of extrapolating a correlation law, if any.

In the following subsections, the non-linear model and the adopted linearization approaches are discussed.

2.1. Engine Thermodynamic Model and Test Conditions

A rotorcraft with a suitable take-off weight for urban air mobility was studied in this paper. The rotorcraft was equipped with a two-spool turboshaft engine, the PW200 Pratt & Whitney Canada, which is developed specifically for helicopter applications. The propulsion system included a free turbine (Low Pressure Turbine (LPT)), connected to the rotor shaft with a nominal speed of 6000 rpm, and a single stage centrifugal compressor driven by a single stage turbine (High Pressure Turbine (HPT)). The specifications for the PW200 are reported in Table 1.

Table 1. PW200 technical specifications.

Description	Value
Power	200–400 [kW]
Weight	110 [kg]
Pressure ratio	8:1
Turbine Inlet temperature	1173.5 [K]
SFC (Specific Fuel Consumption)	0.426–0.33 [kg/kWh]
Compressor Configuration	1 centrifugal
Turbine configuration	HPT, LPT

Due to a lack of experimental data for the selected engine, detailed simulations with GSP software (Gas Turbine Simulation Program) [43] were performed in the present study. The GSP is a tool developed at the Aerospace Department of Delft Technical University, which allows for both transient and steady-state simulations of almost all types of gas turbines (turboshaft, turboprop, turbofan, single and multi-shafts, etc.) by properly establishing a specific arrangement of engine components, and through careful model calibration.

The arrangement of engine components adopted in the present research, which reflects the PW200 configuration, is presented in Figure 1.

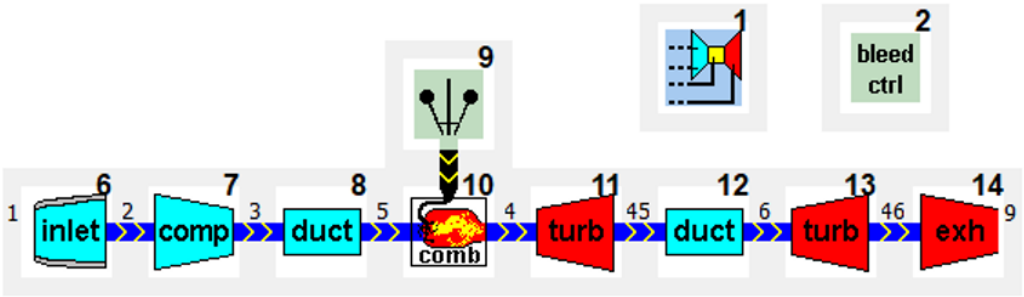

Figure 1. Model of the turboshaft in the GSP.

The model links an inlet (block 6), a compressor (block 7), a combustion chamber (block 10), a high-pressure turbine (block 11) and a low-pressure turbine (block 13) with its exhaust (block 14) connected to the output shaft. Block 1 represents the "manual case control", which changes the desired power, the altitude and the Mach number according to the design of the experiments. Block 2 is the controller of the bleeding air, and block 9 sets the specification of the fuel. Two additional components named "duct" were included in the scheme, and were utilized in transient models to take into account dynamics and volumetric effects, as well as to perform mass balance calculations according to the ICV-Intercomponent Volume method [44,45]. They have no effect on the engine's performance and operational characteristics during steady-state conditions.

As for model calibration, several steps were required:

- The design point, whose main parameters are reported in Table 2, was assumed to be sea-level static (SLS) and at international standard atmospheric (ISA) conditions (temperature = 288.25 K, pressure = 1.013 bar, altitude = 0 m, Mach = 0);
- The default compressor and turbine maps were scaled according to a set of input parameters taken from the database of the reference engine, i.e., intake pressure ratio, design rotor speed, design shaft speed;
- An iteration was run in the GSP by adjusting the design air and fuel flow rates injected into the combustion chamber, in order to obtain the desired power output and SFC. The iteration allowed for an accuracy of 1% in the prediction of take-off power with respect to the design take-off power of the reference engine;
- Using block 1, which allowed for manual case control, the off-design engine variables when changing the operating conditions (desired power, Mach number, altitude) were obtained.

Table 2. PW200 design points.

Description	Value
Power (POW)	295 [kW]
Intake Pressure Ratio (PR)	0.988
Air Flow Rate (W_a)	2 [kg/s]
Compressor pressure ratio (β_c)	7.17
Combustion Efficiency (η_b)	0.985
Fuel Flow Rate (W_f)	0.0315 [kg/s]
Compressor Rotor Speed (N)	40,891 [rpm]
Compressor Efficiency (η_c)	0.825
LPT Rotor Speed (N_{LP})	6000 [rpm]
Turbine Efficiency (η_t)	0.88
Spool Mechanical Efficiency (η_m)	0.99
Mach, Altitude	0, 0

This research examined two mission profiles reported in Figure 2, a simple delivery trip (Mission A for "Transport"), and a search-and-rescue (SAR) mission in a mountain environment (Mission B for "Mountain Rescue"). These missions were also used to generate several points for engine failure, as shown in Table 3.

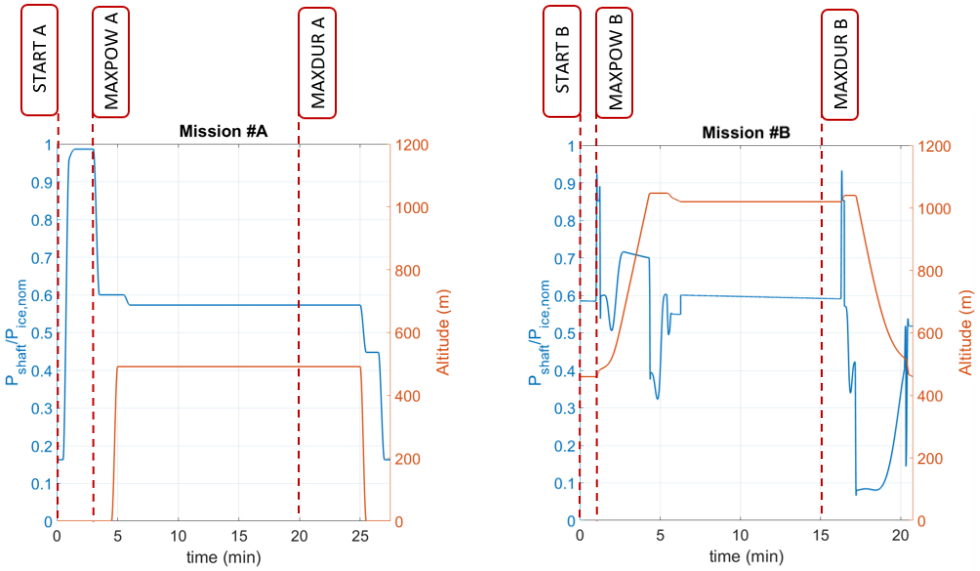

(**a**) (**b**)

Figure 2. Reference missions. (**a**) Mission A for "Transport"; (**b**) Mission B for "Mountain Rescue".

Table 3. Simulated working points.

Description	Speed [m/s]	Altitude [m]	Power [KW]	Low-Pressure Turbine Speed [rpm]
START-A	30.6	0	48	6000
START-B	0	1150	173	6000
MAXPOW-A	30.6	0	291	6000
MAXPOW-B	3.96	1154	273	6000
MAXDUR-A	30.6	492	169	6000
MAXDUR-B	0	2550	176	6000

However, the purpose of the present study relied on the achievement of a linear model of the engine around a working point, which is representative of an equilibrium condition. In particular, the selected operating condition is indicated in Figure 2 as MAXDUR-A, and is characterized by a power lever angle (PLA) of about 50%, altitude h = 50 m and Mach = 0.09. In order to predict the dynamic behavior of the system, the engine equilibrium point must be altered by enforcing small changes to the PLA by applying step, ramp and pulse signals. In this case, variations of ±10% with respect to the steady state value were applied to the PLA according to the sequence displayed in Figure 3; transient simulations, which include dynamic phenomena such as spool inertia, heat transfer in turbomachinery and volumetric effects, were carried out by means of the GSP. The time series data sets obtained from simulations included compressor pressure ratio, compressor rotational speed, inlet and outlet turbine temperature, fuel flow rate, specific fuel consumption, engine torque and power.

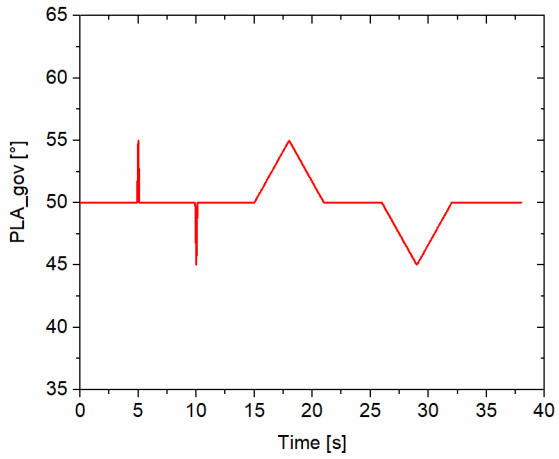

Figure 3. PLA signal.

In the current simulations, the machinery degradation was accounted for. During its life cycle, in fact, an engine undergoes several issues due to over-temperatures, erosion of the compressor and turbine blades, fouling, bird strikes, etc., which contribute to increased machine degradation; as a direct consequence, engine performance reduces. In the literature, these mechanisms cause performance losses approaching 10% in the process [45]. In order to predict the engine performance degradation, the exhaust gas temperature (EGT), which reflects the performance degradation of the aeroengine, is usually monitored and used for engine control, fault diagnosis and maintenance decisions. The GSP allows one to illustrate the engine's deterioration in a variety of ways. The most common method is to conduct a simulation with a continuous degree of degradation, such as continuous reductions in compressor efficiency and mass flow rate. In the current simulations, step changes, represented as a modification of the compressor isentropic efficiency and mass flow parameter, were investigated in order to make the analysis as generic and feasible as possible. The step changes included reductions in compressor efficiency and mass flow parameters amounting to 2%, 4%, 8%, 12% and 15% with respect to healthy conditions. These deterioration levels were still compatible with safe operation of the propeller, as reported in [45,46].

2.2. Linear Model

The primary problem in controller design is to develop a linear model, at the considered operating point of the engine, which can be presented in the following form:

$$\begin{cases} \dot{x} = Ax + Bu \\ y = Cx + Du \end{cases} \quad (1)$$

where $x(t)$ is the state of the model, $u(t)$ is the input variable vector and $y(t)$ is the output vector. A, B, C and D are the linearization matrices. In this formulation, the heat-transfer process can be neglected, owing to the fact that the thermal inertia of the engine components is usually much smaller than that of the rotors [47,48]. Therefore, only the engine shafts dynamics can be taken into account. In addition, in the analyzed engine configuration, the low-pressure turbine shaft is connected to the rotor, which is kept at a constant speed. Hence, the only considered dynamic is the high-pressure turbine shaft rotational speed, N_{HP}. In summary, the state of the system, $x(t)$, is given by the high-pressure turbine shaft speed (N_{HP}); the input vector, $u(t)$, is given by the fuel flow rate (Wf), which, from a controller point of view, is the manipulating variable; and the output vector, $y(t)$, is defined according to physical and structural limits that must be satisfied in the controller design to protect the engine components. These limits include over-pressurization, over-temperature and over-speed, which are controlled by means of some of the following engine performance parameters [34]: the total pressure at the compressor exit (PT_3), the

total temperature at the HPT exit (TT_{45}), the HP shaft speed, N_{HP}, and the shaft power. Therefore, the linear model had 1 input, 4 outputs and 1 state variable, which are fully listed in Table 4.

Table 4. State variables, control inputs and outputs of the desired engine.

State Variables, x	Output Variables, y	Input Variables, u
HP shaft speed, N_{HP} [rpm]	HPC exit total pressure, PT_3 [bar] HPT exit total temperature, TT_{45} [K] HP shaft speed, N_{HP} [rpm] Shaft Power, *Pow* [kW]	Fuel flow, W_f [kg/s]

The approaches proposed for the turboshaft engine dynamic model linearization are discussed in the next subsections.

2.2.1. Perturbation Method

The general form of engine non-linear equations, which include fast and slow dynamics, can be written as follows [31]:

$$\dot{z} = g(x, z, u) \tag{2}$$

$$\dot{x} = f(x, z, u) \tag{3}$$

where z denotes the fast states (mainly flow dynamics), while x denotes the slow states (shaft dynamics, etc.). However, as already mentioned, if it is assumed that the fast dynamics can be neglected and only the high-pressure turbine shaft dynamics is included, only Equation (3) can be considered for linearization purposes. To this aim, an arbitrary position $\overline{x}$, $\overline{z}_0$, $\overline{u}$ is selected, and perturbations (δx,δu) from a linearization point are applied:

$$\dot{x} = f(\overline{x} + \delta x, \overline{z}_0, \overline{u} + \delta u) \tag{4}$$

By differentiating Equation (4) and neglecting the higher order terms, the following equation is obtained:

$$\dot{x} \approx f(\overline{x}, \overline{z_0}, \overline{u}) + \left.\frac{\partial f}{\partial x}\right|_{\overline{x},\overline{z}_0,\overline{u}} \delta x + \left.\frac{\partial f}{\partial u}\right|_{\overline{x},\overline{z}_0,\overline{u}} \delta u \tag{5}$$

As linearization is often achieved about an equilibrium condition where $f(\overline{x}, \overline{z_0}, \overline{u}) = 0$, Equation (5) can be simplified to the following:

$$\dot{x} = A\delta x + B\delta u \tag{6}$$

where $A = [\partial f/\partial x]$ and $B = [\partial f/\partial u]$.

Similarly, the non-linear equations of the output variables are written as follows:

$$y = h(x, z, u) \tag{7}$$

A Taylor approximation is applied to the engine model, Equation (7), at the equilibrium point ($\overline{x}$, $\overline{z}_0$, $\overline{u}$), and the retaining constant and first-order terms yield the following state variable model:

$$y \approx h(\overline{x}, \overline{z_0}, \overline{u}) + \left.\frac{\partial h}{\partial x}\right|_{\overline{x},\overline{z}_0,\overline{u}} \delta x + \left.\frac{\partial h}{\partial u}\right|_{\overline{x},\overline{z}_0,\overline{u}} \delta u = C\delta x + D\delta u \tag{8}$$

where $C = [\partial h/\partial x]$ and $D = [\partial h/\partial u]$ are the system matrices with appropriate dimensions.

The non-linear engine model in the current case included only the conservation of the angular momentum of the high-pressure turbine shaft. The non-linear equation that describes the transient process is given by the following [49]:

$$\dot{N}_{HP} = \frac{\Delta Pow_{HP}}{I_{HP} N_{HP} \left(\frac{2\pi}{60}\right)^2} \tag{9}$$

In the above equation, $\dot{N}_{HP}$ is the angular acceleration of the high-pressure turbine shaft, ΔPow_{HP} is the difference between the power produced by the turbine and the power required by the compressor, and I_{HP} is the moment of inertia of the moving parts of the spool. ΔPow_{HP} is obtained by modeling the compressor and turbine with the help of the machinery maps, which allows the evaluation of pressure, flow rate and efficiency while varying the rotational speed of the components. The correlation between ΔPow_{HP} and fuel flow was obtained by modeling the burner. In fact, fuel flow is a direct input to the burner; inside the combustor, the air and fuel are mixed and burned to produce high temperature gas, which drives the turbine and produces torque. However, the function f, which correlates ΔPow_{HP} to shaft speed and fuel flow, is not explicitly defined in Equation (9). Therefore, the state-space representation of the engine dynamic system can be written as follows:

$$\begin{aligned} \dot{N}_{HP} &= \tfrac{1}{I_{HP}} \times f\left(N_{HP}, W_f\right) \\ y_i &= h\left(N_{HP}, W_f\right) \end{aligned} \tag{10}$$

By applying the small perturbations in the form of Equation (6), the expansion of Equation (10) can be written as follows [34]:

$$\begin{aligned} \Delta\dot{N}_{HP} &= \tfrac{1}{I_{HP}}\left(\tfrac{\partial f}{\partial N_{HP}}\Delta N_{HP} + \tfrac{\partial f}{\partial W_f}\Delta W_f\right) \\ \Delta y_i &= \tfrac{\partial h_i}{\partial N_{HP}}\Delta N_{HP} + \tfrac{\partial h_i}{\partial W_f}\Delta W_f \end{aligned} \tag{11}$$

By a comparison between Equations (6), (8) and (11), it can be observed that the matrices A, B, C and D contain the partial derivatives, and are therefore expressed as follows:

$$\begin{aligned} A &= \left[\tfrac{\partial f}{\partial N_{HP}}\right] \\ B &= \left[\tfrac{\partial f}{\partial W_f}\right] \\ C &= \left[\tfrac{\partial y_1}{\partial N_{HP}} \; \tfrac{\partial y_2}{\partial N_{HP}} \; \tfrac{\partial y_3}{\partial N_{HP}} \; \tfrac{\partial y_4}{\partial N_{HP}}\right] \\ D &= \left[\tfrac{\partial y_1}{\partial W_f} \; \tfrac{\partial y_2}{\partial W_f} \; \tfrac{\partial y_3}{\partial W_f} \; \tfrac{\partial y_4}{\partial W_f}\right] \end{aligned} \tag{12}$$

The values of the partial derivatives were obtained by deviating the input in Equation (11) from its steady value and by collecting, by means of the GSP, the corresponding output and state variables. Their variations, i.e., Δy_i, ΔN_{HP}, ΔW_f, were obtained at each sampling time. Similarly, $\dot{N}_{HP}$ was obtained from finite differences. Therefore, the partial derivatives in Equation (12), which represent the unknown parameters of the system, were obtained through a linear regression over the collected data.

Each linear model was valid only in a neighborhood of an operating point in certain flight conditions (Mach, altitude, weather conditions, etc.). Therefore, in order to develop a controller capable of covering all flight conditions, this procedure had to be repeated for different operating points, and a set of linearized models was collected; hence, piecewise control was implemented.

2.2.2. System Identification

An alternative way to obtain a linear model is based on the adoption of System Identification [40–42]. This methodology is based on a "black-box" approach, in which the mathematical model of a dynamic system is based on observed data. In practice, no

physical details of the non-linear model are needed, only the input/output data of the dynamic system.

System identification requires several steps, which can be summarized as follows:

- Attaining input/output data of the dynamic system;
- Selecting a suitable linear model structure from among discrete/continuous transfer functions or state-space forms;
- Fitting a suitable linear model to data and considered model structure;
- Verifying whether the model is good enough to represent the system.

As for the input/output data (a), these could be collected by means of experimental data or through a valid simulation tool. Concerning the linear model structure (b), the state-space form is usually preferable for the design of the controller. The linear model fitting (c) is usually available in various computational tools; in this case, it was carried out using the system identification toolbox of MATLAB [49]. Finally, a number of validation tests were available from the literature (d); these included correlation tests, one-step ahead prediction, model-predicted output, estimation, and test data.

From the literature [34], it was expected that the system identification approach would provide better results in terms of percentages of compliance to the experimental data with respect to the perturbation approach. However, since the linearization procedure was the result of a best fitting procedure, the drawback of the SI was that it relied on the loss of a physical meaning of the matrices elements, which had a relevant impact on the development of the controller, as will be discussed below.

3. Results and Discussion

In this section, a comparison between the proposed approaches for system linearization to a case study is presented. The case study was based on a simple delivery trip, in which the operating equilibrium conditions were characterized by a power lever angle (PLA) of about 50%, altitude h = 50 m and Mach = 0.09 (Figure 2). The dynamic behavior of the system was predicted in GSP software for different degradation levels of the compressor through the application of step, ramp and pulse signals to the PLA (Figure 3).

For each perturbation of the PLA around the equilibrium condition, the small perturbation and system identification approaches were applied to linearize the engine model. For both approaches, the input/output data and the state variables, obtained from simulations carried out by means of GSP software, were used for the estimation of the matrix coefficients of the linear model during the dynamic maneuvers. For the perturbation method, the matrix coefficients were obtained through a linear regression, whereas the system identification method obtained these by means of the MATLAB toolbox. Both methods allowed for prediction of the output engine variables with different levels of compressor degradation.

In order to assess the accuracy of linearization, the maximum error percentage, *MaxErr*, the mean error percentage, *MeanErr* and the coefficient of determination, R^2, were defined as follows:

$$\begin{aligned} MaxErr &= \frac{max(|Y_{GSP} - Y_{LM}|)}{max(|Y_{GSP}|)} \times 100 \\ MeanErr &= \frac{\frac{\sum_{i=1}^{N}(|Y_{GSP}(i) - Y_{LM}(i)|)}{N}}{max(|Y_{GSP}|)} \times 100 \\ R^2 &= 1 - \frac{\sum_{i=1}^{N}(Y_{GSP}(i) - Y_{LM}(i))^2}{\sum_{i=1}^{N}(Y_{GSP}(i))^2 - \frac{\left(\sum_{i=1}^{N} Y_{LM}(i)\right)^2}{N}} \end{aligned} \quad (13)$$

In Equation (13), Y_{GSP} is the output signal from the non-linear GSP model, Y_{LM} is the output signal from the linear model, and N represents the number of sampling times.

3.1. Linearized Turboshaft Model with Perturbation Method

Table 5 summarizes the comparison between the linear model and the GSP data for the output variables for the different levels of compressor degradation and flow coefficient, for the engine operating at the point previously indicated as MaxDurA (Table 3). It can

be observed that the linear model predicts the output variables with high accuracy. The results show that the mean error was below 1% for all of the output variables, and that the maximum error, which was lower than 6%, was recorded for shaft power. These values, which can be considered excellent according to the literature [34], allowed us to conclude that the linear model obtained through the perturbation method provides optimal predictive capabilities.

Table 5. Linear model validation.

OUTPUTVAR. / DEGRAD. LEVEL	PT_3 [bar]			TT_{45} [K]			Power [kW]		
	Mean Err. %	Max Err. %	R^2	Mean Err. %	Max Err. %	R^2	Mean Err. %	Max Err. %	R^2
Clean	0.08	1.36	0.994	0.06	3.46	0.968	0.23	5.81	0.987
2%	0.07	1.39	0.995	0.06	3.40	0.969	0.23	5.86	0.987
4%	0.07	1.48	0.994	0.06	3.37	0.971	0.23	5.99	0.987
8%	0.07	1.51	0.994	0.06	3.24	0.973	0.24	5.97	0.987
12%	0.07	1.49	0.994	0.06	3.12	0.975	0.24	5.92	0.988
15%	0.07	1.48	0.995	0.06	3.00	0.976	0.24	5.88	0.988

Figure 4 shows the results of the linear model for the clean and damaged compressor at two different levels of compressor degradation and flow coefficient (8 and 12%, respectively), when small PLA perturbations were enforced according to Figure 3. For each case, a sudden increase in fuel flow rate caused a rise in turbine exhaust gas temperature (Figure 4a) and turbine speed (Figure 4b), and, consequently, a higher power at the turbine shaft (Figure 4c). The higher shaft speed increased the compressor pressure ratio, as shown in Figure 4d. The inverse behavior for the same output variables was obtained when the fuel flow rate was reduced.

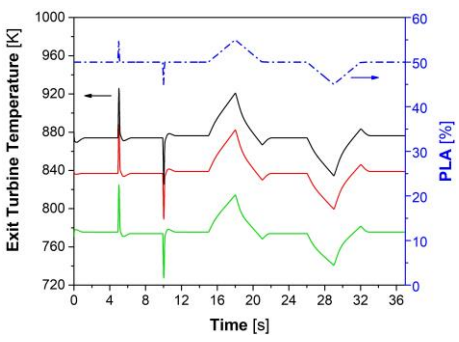

(**a**)

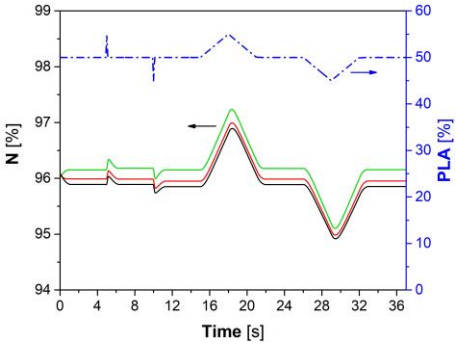

(**b**)

Figure 4. *Cont.*

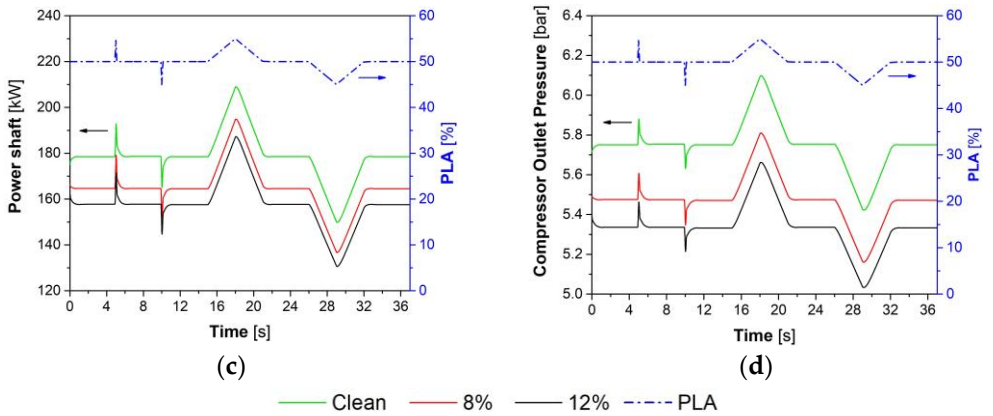

Figure 4. Comparison between the GSP and linear model output variables. (**a**) Exhaust gas temperature; (**b**) shaft speed; (**c**) shaft power; (**d**) compressor outlet pressure. The black arrow indicates the primary axis variables; the blue arrow refers to the secondary axis (PLA).

The linearization matrices of Equation (12) were computed for each of the analyzed cases, and the coefficients of matrices A, B, C and D were plotted in Figures 5–8, respectively. It can be observed that the trend of each coefficient, with increasing the compressor degradation level, is approximately linear for most of the cases. This is a very interesting and favorable occurrence from a controller point of view, as it allows one to implement, for each matrix element, a linear law with the health status of the component. These laws, together with the R^2, are summarized in Table 6.

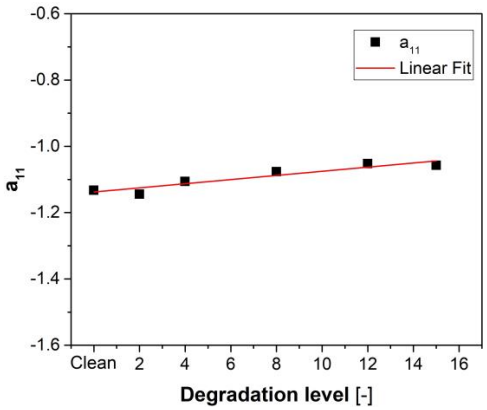

Figure 5. Coefficient a_{11} computed from linearization for different levels of compressor degradation (dots) and the linear fit curve.

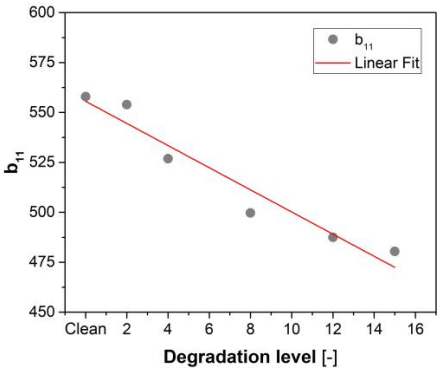

Figure 6. Coefficient b_{11} computed from linearization for different levels of compressor degradation (dots) and the linear fit curve.

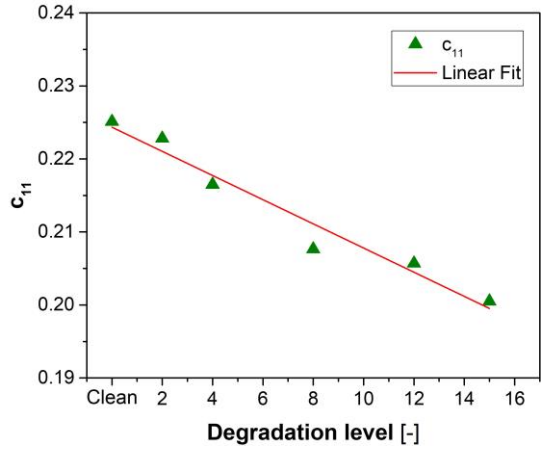

Figure 7. Coefficient c_{11} of Matrix C computed from linearization for different levels of compressor degradation (dots) and the linear fit curve.

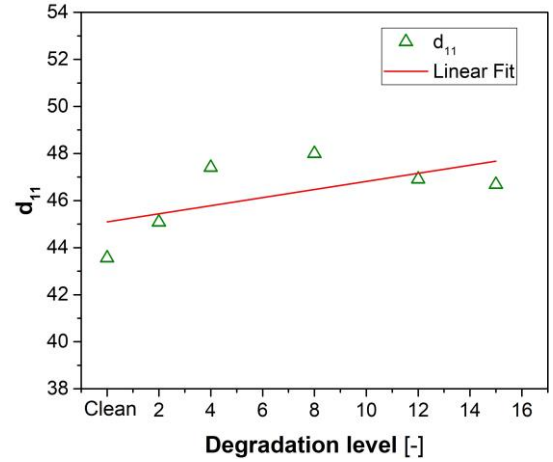

Figure 8. Coefficient d_{11} of Matrix D computed from linearization for different levels of compressor degradation (dots) and the linear fit curve.

Table 6. Matrices linear laws with degradation degree, *h*.

Matrix Coefficient	Linear Law	R^2
a_{11}	$a_{11} = 0.003h - 1.129$	0.862
b_{11}	$b_{11} = -5.912h + 562.5$	0.902
c_{11}	$c_{11} = -0.002h + 0.225$	0.981
c_{21}	$c_{21} = -9.52h - 0.278$	0.998
c_{31}	$c_{31} = -0.179h + 27.28$	0.929
c_{41}	$c_{41} = -0.111h + 16.972$	0.929
d_{11}	$d_{11} = 0.134h + 44.96$	0.853
d_{21}	$d_{21} = 198.5h + 17,714$	0.994
d_{31}	$d_{31} = 9.526h + 8047.3$	0.778
d_{41}	$d_{41} = 6.749h + 4999.7$	0.739

As Equation (11) shows, each term of the linearization matrices represents a physical property of the aero-engine system. As for Equation (11), for instance, a_{11} represents the time constant of the engine through the correlation $\tau = -\frac{1}{a_{11}}$ [12]. Hence, a_{11} was expected to be negative; moreover, with increasing compressor degradation, a_{11} increased (Figure 6). This indicates that, as expected, a damaged compressor contributes to retarding the time of response of the shaft. As for b_{11}, this coefficient correlates the shaft acceleration to a fuel flow rate variation. Therefore, when an increase in fuel flow rate is applied, a shaft

acceleration is expected. When the compressor is damaged, the higher the degradation level, the slower the shaft accelerates. The linear trend is observed in Figure 6.

As for the output equation (Equation (11)), the terms of matrices C and D are the partial derivatives of each output variable, and represent the slopes of a small change in the output variable with respect to a small change in the state variable, N_{HP}, and with respect to a small change in the input variable, W_f, respectively. These coefficients varied with the level of degradation of the compressor, as plotted in Figures 7 and 8. For instance, with reference to c_{11}, which represents the rate of change in compressor pressure PT_3 to a small variation in shaft speed, it is clear that by increasing the shaft speed, the compressor outlet pressure increases accordingly; therefore, $c_{11} > 0$. If the compressor is damaged, the same increase in shaft speed corresponds to a lower pressure rise. This was confirmed by the decreasing trend in c_{11}, as displayed in Figure 7. Similar considerations can be made for the other coefficients.

Finally, the achieved results allowed us to carry out an analysis on the effects of engine degradation on the output variables. A steady-state operating condition, in which fuel flow rate and engine speed were fixed (fixed PLA), was considered for different values of compressor degradation. Figure 9 (top) shows that the more the compressor was damaged, the lower the pressure and the higher the air temperature at the compressor exit. In particular, an efficiency drop of 8% caused a pressure reduction of about 4% and a temperature rise of 2.8%; if the compressor efficiency dropped by 12%, then the pressure reduced by about 7% and the temperature increases by about 4.5%. When the compressor is damaged, its performance map undergoes considerable changes. Therefore, at a fixed speed, lower air flow rates were processed by the compressor with respect to the clean case. Air flow rates reductions of about 8% and 12% with respect to the clean case were recorded for compressor efficiency reductions of about 8% and 12%, respectively. The lower air flow rates, at fixed fuel, caused a rise in the turbine inlet and exhaust temperature (Figure 10). Therefore, for a compressor degradation of about 8%, the inlet and outlet turbine temperatures rose by about 7%, while for a compressor degradation of about 12%, the temperatures rose by about 10%. Overall, engine performance deteriorated and lower power was obtained, as reported in Table 7. These results are in agreement with the literature data [46,50].

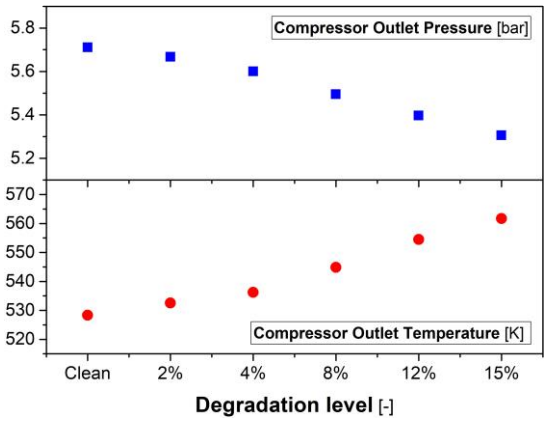

Figure 9. Compressor pressure (**top**) and outlet compressor temperature (**bottom**) for damaged compressor.

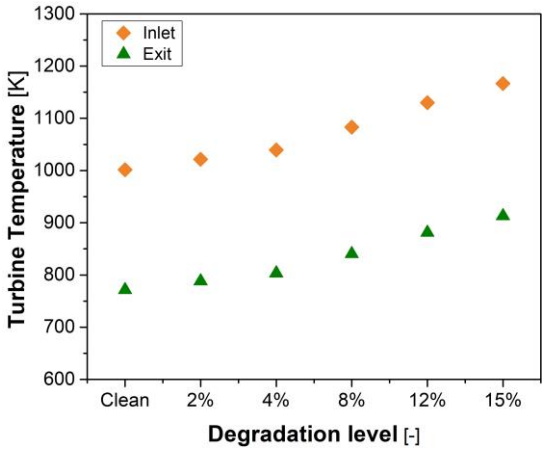

Figure 10. Turbine inlet and exit temperatures for damaged compressor.

Table 7. Power reduction with increasing compressor degradation for operating point (PLA) of about 50%, altitude h = 50 m and Mach = 0.09, at 6000 rpm.

Degradation	Output Power [kW]	% Power Variation
clean	178	
2%	175	−1.7
4%	171	−3.9
8%	164	−7.9
12%	157	−11.8
15%	152	−14.6

3.2. Linearized Turboshaft Model with System Identification (SI)

The model linearization was carried out through the Matlab System Identification toolbox. In this case, the input and output data vectors were given to the software using a GUI, and the state-space model was selected from among the available ones (transfer functions, polynomial, non-linear and other dynamic models). Two algorithms for SI are available: SSEST, which allows for the estimation of a continuous-time state-space model, and N4SID, which allows for the definition of a discrete-time state space model. In the latter case, the discrete-time identified state-space model has the following form:

$$\begin{aligned} x(t+T_s) &= Ax(t) + Bu(t) + Ke(t) \\ y(t) &= Cx(t) + Du(t) + e(t) \end{aligned} \tag{14}$$

where A, B, C, D and K are state-space matrices, $u(t)$ is the input, $y(t)$ is the output, $e(t)$ is the disturbance and $x(t)$ is the vector of n_x states, which represent the order of the system. In the present case, the N4SID algorithm with n_x = 4 was selected. It is worth pointing out that n_x = 4 was selected on the basis of a trial-and-error approach in order to achieve the best agreement between the linear model output and the experiments. Moreover, this procedure does not require the definition of the state variables, only their order (four in this case). Therefore, the physical meaning of the matrices elements, which were obtained by adopting the small perturbation approach, were lost in this case.

The comparison between the SI output variables and the GSP results is included in Table 8. It can be observed that by adopting this approach, the mean error was also below 1% for all of the output variables; moreover, a maximum error lower than 3%was recorded for the shaft power. The values of this approach were even better than those for the previous approach; therefore, similarly to the previous approach, these results allow one to conclude that the linear model obtained through the SI provides optimal predictive capabilities.

Table 8. Linear model validation.

OUTPUTVAR. / DEGRAD. LEVEL	PT_3 [bar]			TT_{45} [K]			Power [kW]		
	Mean Err. %	Max Err. %	R^2	Mean Err. %	Max Err. %	R^2	Mean Err. %	Max Err. %	R^2
Clean	0.08	1.08	0.995	0.04	0.19	0.999	0.10	0.30	0.999
2%	0.08	0.83	0.997	0.04	0.27	0.999	0.10	0.32	0.999
4%	0.09	0.67	0.997	0.05	0.26	0.998	0.11	0.33	0.999
8%	0.13	0.91	0.991	0.06	0.49	0.997	0.22	2.08	0.997
12%	0.10	0.95	0.997	0.07	0.61	0.996	0.22	2.29	0.997

Matrices A, B, C and D, for the analyzed case, had the following dimensions: 4×4, 4×1, 4×4 and 4×1, respectively. As in the previous case, each term of the matrices was analyzed with varying the compressor degradation level, in order to extrapolate a degradation law. Unfortunately, the coefficients varied in an unpredictable manner. For each term, the R^2 was computed, and this clearly indicated the poor fitting of the data with a linear trend. This allows one to conclude that this approach is not suitable for implementation in controller design when prediction of components degradation is included.

4. Conclusions

In this study, two approaches for obtaining reliable linear models of a turboshaft aircraft engine were analyzed. The main purpose of developing such linear models relied on the possibility of developing advanced control systems for direct fuel control instead of adopting measurable parameters. Moreover, the possibility of including components degradation in the linear model, in order to reduce control correction error, was investigated. The adopted techniques were Small Perturbation and System Identification. The models were validated by a comparison with simulation results, under the same operating conditions, obtained through a high-fidelity simulation tool (GSP).

Both approaches yielded quite reliable results in predicting the output variables for all of the degradation conditions. In fact, from a comparison between the linear model and data, the Small Perturbation approach yielded a recorded mean error below 1% for all of the output variables, and the maximum error, recorded for shaft power, was about 6%. For System Identification, even better results were obtained. In fact, the mean error was below 1% for all of the output variables, and the maximum error, recorded in this case for shaft power, was lower than 3%.

A simple correlation between engine performance and components degradation was also demonstrated; in particular, the achieved results allow one to conclude that the Small Perturbation approach is the best candidate for controller development when a prediction of components degradation is included.

Author Contributions: Conceptualization, T.C., A.F. and S.B.; methodology, A.F. and T.C.; software, D.P. and L.S.; validation, L.S. and D.P.; resources, D.P. and L.S.; data curation, T.C.; writing—original draft preparation, T.C.; writing—review and editing, T.C. and A.F.; supervision, S.B. and A.F.; project administration, A.F.; funding acquisition, A.F. All authors have read and agreed to the published version of the manuscript.

Funding: This research was funded by the Italian Ministry of University and Research, Project PON "SMEA", Cod. PON03PE_00067_5 CUP: B74C12000310005.

Data Availability Statement: The data used in this paper are publicly available from the sources cited in the text.

Conflicts of Interest: The authors declare no conflict of interest.

References

1. Élimination des Émissions Nettes de Carbone d'ici 2050 IATA COMMUNIQUÉ No: 66. Available online: https://www.iata.org/contentassets/dcd25da635cd4c3697b5d0d8ae32e159/2021-10-04-03-fr.pdf (accessed on 1 December 2022).
2. Flamm, J.; James, K.; Bonet, J. Overview Of ERA Integrated Technology Demonstration (ITD) 51A Ultra-High Bypass (UHB) Integration for Hybrid Wing Body (HWB). In Proceedings of the 54th AIAA Aerospace Sciences Meeting, San Diego, CA, USA, 4–8 January 2016.
3. Donateo, T.; De Pascalis, C.L.; Strafella, L.; Ficarella, A. Off-line and On-line Optimization of the Energy Management Strategy in a Hybrid Electric Helicopter for Urban Air-Mobility. *Aerosp. Sci. Technol.* **2021**, *113*, 106677. [CrossRef]
4. Dinc, A. NOx Emissions of Turbofan Powered Unmanned Aerial Vehicle for Complete Flight Cycle. *Chin. J. Aeronaut.* **2020**, *33*, 1683–1691. [CrossRef]
5. Cabrera, E.; de Sousa, J.M.M. Use of Sustainable Fuels in Aviation—A Review. *Energies* **2022**, *15*, 2440. [CrossRef]
6. Montazeri-Gh, M.; Rasti, A.; Jafari, A.; Ehteshami, M. Ehteshami, Design and Implementation of MPC for Turbofan Engine Control System. *Aerosp. Sci. Technol.* **2019**, *92*, 99–113. [CrossRef]
7. Wei, Z.; Jafari, S.; Zhang, S.; Nikolaidis, T. Hybrid Wiener model: An On-board Approach Using Post-Flight Data for Gas Turbine Aero-Engines Modelling. *Appl. Therm. Eng.* **2021**, *184*, 116350. [CrossRef]
8. Sun, X.; Jafari, S.; Fashandi, S.A.M.; Nikolaidis, T. Compressor Degradation Management Strategies for Gas Turbine Aero-Engine Controller Design. *Energies* **2021**, *14*, 5711. [CrossRef]
9. Imani, A.; Montazeri-Gh, M. Improvement of Min–Max Limit Protection in Aircraft Engine Control: An LMI approach. *Aerosp. Sci. Technol.* **2017**, *68*, 214–222. [CrossRef]
10. Mohammadi, E.; Montazeri-Gh, M. Active Fault Tolerant Control with Self-Enrichment Capability for Gas Turbine Engines. *Aerosp. Sci. Technol.* **2016**, *56*, 70–89. [CrossRef]
11. Chen, Y.; Guo, Y.; Li, R. State Feedback Control for Partially Distributed Turboshaft Engine with Time Delay and Packet Dropouts. In Proceedings of the 37th Chinese Control Conference, Wuhan, China, 25–27 July 2018; pp. 25–27.
12. Mattingly, J.; Jaw, L. *Aircraft Engine Controls: Design, System Analysis, and Health Monitoring*, 1st ed.; AIAA: Reston, VA, USA, 2009.
13. Connolly, J.W.; Csanky, J.; Chicatelliz, A. Advanced Control Considerations for Turbofan Engine Design. In Proceedings of the 52nd AIAA/SAE/ASEE Joint Propulsion Conference, Salt Lake City, UT, USA, 25–27 July 2016; pp. 1–18.
14. Lu, F.; Qian, J.N.; Huang, J.; Qiu, X. In-flight Adaptive Modeling using Polynomial LPV Approach for Turbofan Engine Dynamic Behavior. *Aerosp. Sci. Technol.* **2017**, *64*, 223–236. [CrossRef]
15. Castiglione, T.; Morrone, P.; Perrone, D.; Bova, S. Application of a model-based controller for improving internal combustion engines fuel economy. *Energies* **2020**, *13*, 1148. [CrossRef]
16. DeCastro, J. Rate-based Model Predictive Control of Turbofan Engine Clearance. *J. Propuls. Power* **2007**, *23*, 804–813. [CrossRef]
17. Zheng, Q.; Xu, Z.; Zhang, H.; Zhu, Z. A Turboshaft Engine NMPC Scheme for Helicopter Autorotation Recovery Maneuver. *Aerosp. Sci. Technol.* **2018**, *76*, 421–432. [CrossRef]
18. Peng, K.; Fan, D.; Yang, F.; Fu, Q.; Li, Y. Active Generalized Predictive Control of Turbine Tip Clearance for Aero-Engines. *Chin. J. Aeronaut.* **2013**, *26*, 1147–1155. [CrossRef]
19. Pang, S.; Li, Q.; Ni, B. Improved Nonlinear MPC for Aircraft Gas Turbine Engine Based on Semi-Alternative Optimization Strategy. *Aerosp. Sci. Technol.* **2021**, *118*, 106983. [CrossRef]
20. Yin, K.; Zhou, W.X.; Qiao, K.; Wang, H.J. Research on Methods of Improving Real-time Performance for Aero-engine Component-level Model. *J. Propuls. Technol.* **2017**, *38*, 199–206.
21. Junior, H.G.; Bringhenti, C.; Barbosa, J.R.; Tomita, J.T. Real-time Gas Turbine Model for Performance Simulations. *J. Aerosp. Technol. Manag.* **2017**, *9*, 346–356. [CrossRef]
22. Lu, J.; Guo, Y.Q.; Zhang, S.G. Research on the Iteration Methods in Aero-Engine Non-Linear Model Real-Time Computation. *J. Aerosp. Power* **2010**, *25*, 681–686.
23. Khorasani, K.; Kiakojoori, S. Dynamic Neural Networks for Gas Turbine Engine Degradation Prediction, Health Monitoring and Prognosis. *Neural Comput. Appl.* **2016**, *27*, 2157–2192. [CrossRef]
24. De Giorgi, M.G.; Quarta, M. Hybrid MultiGene Genetic Programming—Artificial Neural Networks Approach for Dynamic Performance Prediction of an Aeroengine. *Aerosp. Sci. Technol.* **2020**, *103*, 105902. [CrossRef]
25. Asgari, H.; Chen, X.; Morini, M.; Pinelli, M.; Sainudiin, R.; Spina, P.; Venturini, M. NARX Models for Simulation of the Start-Up Operation of a Single-Shaft Gas Turbine. *Appl. Therm. Eng.* **2016**, *93*, 368–376. [CrossRef]
26. Zheng, Q.; Pang, S.; Zhang, H.; Hu, Z. A study on Aero-Engine Direct Thrust Control with Nonlinear Model Predictive Control Based on Deep Neural Network. *Int. J. Aeronaut. Space Sci.* **2019**, *20*, 933–939. [CrossRef]
27. Du, X.; Sun, X.-M.; Wang, Z.-M.; Dai, A.-N. A Scheduling Scheme of Linear Model Predictive Controllers for Turbofan Engines. *IEEE Access* **2017**, *5*, 24533–24541. [CrossRef]
28. Du, X.; Guo, Y.Q.; Chen, X.L. Multivariable Constrained Predictive Control and its Application to a Commercial Turbofan Engine. *Adv. Mater. Res.* **2014**, *99*, 281–287. [CrossRef]
29. Saluru, D.; Yedavalli, R.; Belapurkar, R. Active Fault Tolerant Model Predictive Control of a Turbofan Engine Using C-MAPPS40k. In Proceedings of the Asme 5th Annual Dynamic Systems and Control Division Conference and JSME 11th Motion and Vibration Conference, Fort Lauderdale, FL, USA, 17–19 October 2012; pp. 349–358. [CrossRef]

30. Sugiyama, N. Derivation of System Matrices From Nonlinear Dynamic Simulation of Jet Engines. *J. Guid. Control. Dyn.* **1994**, *17*, 1320–1326. [CrossRef]
31. Chung, G.; Prasad, J.; Dhingra, M.; Meisner, R. Real Time Analytical Linearization of Turbofan Engine Model. *ASME J. Eng. Gas Turbines Power* **2014**, *136*, 011201. [CrossRef]
32. Kulikov, G.; Thompson, H. *Dynamic Modelling of Gas Turbines: Identification, Simulation, Condition Monitoring and Optimal Control*; Springer: London, UK, 2004.
33. Armstrong, J.; Simon, D. *Constructing an Efficient Self-Tuning Aircraft Engine Model for Control and Health Management Applications*; Report No.: NASA/TM- 2012-217806; Glenn Research Center, National Aeronautics and Space Administration: Cleveland, OH, USA, 2012.
34. Montazeri-Gh, M.; Rasti, A. Analyzing Different Numerical Linearization Methods for the Dynamic Model of a Turbofan Engine. *Mech. Ind.* **2019**, *20*, 303. [CrossRef]
35. Luppold, R.; Roman, J.; Gallops, G.; Kerr, L. Estimating In-Flight Engine Performance Variations Using Kalman Filter Concepts. In Proceedings of the AIAA/ASME/SAE/ASEE 25th Joint Propulsion Conference, Monterey, CA, USA, 10–12 July 1989; p. 2584.
36. Simon, D.; Garg, S. Optimal Tuner Selection For Kalman Filter-Based Aircraft Engine Performance Estimation. *J. Eng. Gas Turbines Power* **2009**, *132*, 031601. [CrossRef]
37. Csank, J.; Connolly, J. Model-Based Engine Control Architecture with An Extended Kalman Filter. In Proceedings of the AIAA Guidance, Navigation, and Control Conference, San Diego, CA, USA, 4–8 January 2016.
38. Nayfeh, A. *Perturbation Methods*; Wiley-VCH Verlag GmbH & Co. KGaA: Weinheim, Germany, 2004.
39. Holmes, M. *Introduction to Perturbation Methods*, 2nd ed.; Springer Science+Business Media: New York, NY, USA, 2013.
40. Tavakolpour-Saleh, A.; Nasib, S.; Sepasyan, A.; Hashemi, S. Parametric and Nonparametric System Identification of an Experimental Turbojet Engine. *Aerosp. Sci. Technol.* **2015**, *43*, 21–29. [CrossRef]
41. Ljung, L. *System Identification—Theory for the User*, 2nd ed.; Printice Hall: Hoboken, NJ, USA, 1999.
42. Keesman, K.J. *System Identification—An Introduction*; Springer: London, UK, 2011.
43. GSP 11 User Manual National Aerospace Laboratory NLR 2016. Available online: https://www.gspteam.com/Files/manuals/UM/GSP_UM_11.pdf (accessed on 1 July 2021).
44. Janikovic, J. Gas Turbine Transient Performance Modeling for Engine Flight Path Cycle Analysis. Ph.D. Thesis, Cranfield University, Bedford, UK, 2010.
45. Sogut, M.Z.; Yalcin, E.; Karakoc, T.H. Assessment of degradation effects for an aircraft engine considering exergy analysis. *Energy* **2017**, *140*, 141–1426. [CrossRef]
46. Kurz, R.; Brun, K. Degradation in Gas Turbine Systems. *ASME J. Eng. Gas Turbines Power* **2001**, *123*, 70–77. [CrossRef]
47. Zhao, N.-B.; Yang, J.-L.; Li, S.-Y.; Sun, Y.-W. A GM (1, 1) Markov Chain-Based Aeroengine Performance Degradation Forecast Approach Using Exhaust Gas Temperature. *Math. Probl. Eng.* **2014**, *2014*, 832851. [CrossRef]
48. DeCastro, J.; Litt, J.; Frederick, D. A Modular Aero-Propulsion System Simulation Of A Large Commercial Aircraft Engine. In Proceedings of the 44th AIAA/ASME/SAE/ASEE Joint Propulsion Conference and Exhibit, Hartford, CT, USA, 21–23 July 2008.
49. *Matlab Users Guide*; University of New Mexico: Albuquerque, NM, USA, 1982.
50. Igie, U.; Goiricelaya, M.; Nalianda, D.; Minervino, O. Aero engine compressor fouling effects for short- and long-haul missions. *Proc. Inst. Mech. Eng. Part G J. Aerosp. Eng.* **2016**, *230*, 1312–1324. [CrossRef]